molecules

MDPI

Article

The Sorption Performance of Cetyl Trimethyl Ammonium Bromide-Capped $La_{0.9}Sr_{0.1}FeO_3$ Perovskite for Organic Pollutants from Industrial Processes

Shimaa M. Ali [1,2,*] and Areej A. Eskandrani [2]

[1] Chemistry Department, Faculty of Science, Cairo University, Giza 12613, Egypt
[2] Chemistry Department, Faculty of Science, Taibah University, Medinah 30002, Saudi Arabia; a.eskandrani@gmail.com
* Correspondence: sali@sci.cu.edu.eg; Tel.: +966-556793098

Received: 5 February 2020; Accepted: 31 March 2020; Published: 2 April 2020

Abstract: $La_{0.9}Sr_{0.1}FeO_3$ perovskite, prepared by the microwave-assisted method, was capped with cetyl trimethyl ammonium bromide (CTAB) cationic surfactant, and applied as a sorbent for the removal of the anionic Congo red (CR) dye from aqueous solutions. X-ray diffraction (XRD) patterns showed that the perovskite structure was not affected by capping; however, the particle size increased. There was a hipsochromic shift in the value of λ_{max} of the CR absorption spectrum in the presence of CTAB, which indicated the formation of an oppositely charged dye–surfactant complex. The adsorption efficiency of CTAB-capped $La_{0.9}Sr_{0.1}FeO_3$ was independent of the pH of the solution—equilibrium was reached after a few minutes. The value of the maximum adsorption capacity, q_m, was 151.52 mg·g^{-1}, which was 10-times higher than that of the pure perovskite. The proposed sorbent maintained its excellent sorption ability in the presence of the sample matrix; therefore, it can be regenerated and reused with unchanged performance.

Keywords: Ternary perovskites; surfactant; capping; adsorption; Congo red dye; water decontamination

1. Introduction

Surfactants are organic compounds that can be used to decrease the surface tension of liquids. A surfactant consists of both hydrophilic (heads) and hydrophobic (tails) groups; therefore, it can be used in detergents, wetting and foaming agents, dispersants, etc. It can be classified according to the charge of its hydrophilic groups into cationic, anionic, non-ionic, and Zwitter-ionic surfactants [1]. Surfactants have various important applications in many fields, they can be added during the synthesis of nanoparticles to prevent coagulation, since they act as a stabilizer. This is particularly important in the synthesis of magnetic nanoparticles [2–5]. Surfactants and their composites can be used for water and wastewater decontamination, where they can be used to remove oppositely charged toxic metal ions and organic compounds via strong electrostatic attractions [6–8]. They can also be used for the corrosion protection of metals that can from an oxide layer, where surfactants can be adsorbed onto the oxide layer, providing a protective coating for the metal [9–11]. Surfactants were also used to improve the electrochemical sensing performance of many compounds and drugs [12–15] and catalytic processes [16–20].

Perovskites are mixed nano-oxides of the general formula ABO_3, where A is a lanthanide or an alkali earth metal and B is a transition metal. Perovskites are interesting materials because a wide range of properties can result from a large number of possible metal ion combinations that can form the

perovskite structure [21,22]. Perovskites have several important applications, for example in catalysis, sensors [23–25], and as sorbents for water decontamination [26–28].

Organic dyes constitute a major source of pollution in wastewater produced from many industries, which poses a threat to the water quality and the life of living beings [29]. The removal of organic dyes using perovskite sorbents was reported in the literature. $SrTiO_3$ nanoparticles were used for the removal of the anionic congo red (CR) [30], and the cationic malachite green dye [31]. Silica-coated $LaMnO_3$ perovskite was used for the removal of cationic methylene blue and anionic methyl orange dyes [32]. $La_{0.5}Pb_{0.5}MnO_3$ [33] and $La_{0.5}Ca_{0.5}NiO_3$ [34] were used for the removal of Eosin dye and reactive blue, respectively.

Cetyl trimethyl ammonium bromide (CTAB) is a cationic surfactant, CTAB-modified materials can be used for the removal of the anionic CR dye from aqueous solutions, such as CTAB/chitosan [35], CTAB/chitosan hydrogel beads [36], CTAB/tea waste [37], CTAB/hectorite [38], CTAB/kaolin [39], CTAB/bentonite [40], and CTAB/graphene oxide [41].

Most perovskites have a negative charge under neutral conditions [26]; therefore, a cationic surfactant can be easily adsorbed onto the perovskite surface and used for the removal of negatively charge ions or anionic dyes from water. The combination of CTAB and perovskites has not been previously reported. Therefore, in this work, $La_{0.9}Sr_{0.1}FeO_3$ perovskite, prepared by the microwave-assisted method, will be capped by CTAB and then employed as an adsorbent for CR dye from aqueous solutions and real samples. Factors affecting the adsorption process such as pH, contact time, initial dye concentration, and temperature will be studied and optimized. The sorption performance of CTAB-capped $La_{0.9}Sr_{0.1}FeO_3$ perovskite is compared with the pure perovskite and with other reported CTAB-capped materials. A method for the sorbent regeneration and reuse is examined.

2. Results and Discussions

2.1. Characterization of CTAB-capped $La_{0.9}Sr_{0.1}FeO_3$ Perovskite

Structural characterizations of pure and CTAB-capped $La_{0.9}Sr_{0.1}FeO_3$ perovskites were carried out by XRD and FTIR, to show the effect of surfactant capping on the perovskite structure and to prove that the modification was successfully performed. Figure 1A shows XRD patterns of pure and CTAB-capped samples. Similar XRD patterns were noticed for both samples, indicating that surfactant capping did not affect the perovskite structure. By comparing data to the standard $LaFeO_3$, ICDD card number: 88-641, all diffraction peaks were indexed to corresponding planes, as indicated in Figure 1A.

The phase identification showed that a single orthorhombic phase of $LaFeO_3$ was formed, with higher d-values than those of the standard $LaFeO_3$ sample. This was due to the partial replacement of the smaller La^{3+} ions with the larger Sr^{2+} ions [26]. However, two differences can be observed between XRD spectra of pure and CTAB-capped perovskites, peaks were narrower and shifted to higher d-values due to the surfactant modification, which indicated that the particle size is higher in the CTAB-capped sample compared to that in pure CTAB. The calculated average particle sizes, using the Schererr equation [42] were 30.8, 45.3 nm, for pure and CTAB-capped samples, respectively. The second difference is the lower peak intensities in the case of the CTAB-capped sample, which indicated that there was an interaction between the perovskite and CTAB, this interaction was also indicated in the FTIR data.

Figure 1B shows FTIR spectra of pure and CTAB-capped $La_{0.9}Sr_{0.1}FeO_3$ perovskites. The characteristic Fe-O stretching band of the perovskite FeO_6 octahedral group appeared in both samples at 559 cm^{-1} [26]. Furthermore, a strong band at 3404 cm^{-1} can be observed, which was assigned to the O-H stretching vibration of adsorbed water. Additional bands at 2918 and 2850 cm^{-1} appeared only in the FTIR spectrum of the CTAB-capped sample. These bands were due to the C-H stretching vibration of $-CH_3$ and $-CH_2$ groups of CTAB, respectively. A weak band appeared at 1468 cm^{-1}, which was assigned to N^+-CH_3 absorption—this band had a strong signal in the FTIR spectrum of pure CTAB [6,43]. However, in the case of the CTAB-capped perovskite FTIR spectrum, the intensity

of this band was weak, which indicated that there was an interaction between the perovskite and CTAB through its ammonium moiety. The appearance of these bands proved that the CTAB surfactant modification of $La_{0.9}Sr_{0.1}FeO_3$ perovskite was successful. At a pH value > the point of zero charge, the perovskite acquired negative charges, which can attract the ammonium moieties in CTAB, resulting in the CTAB-capped perovskite [26,31].

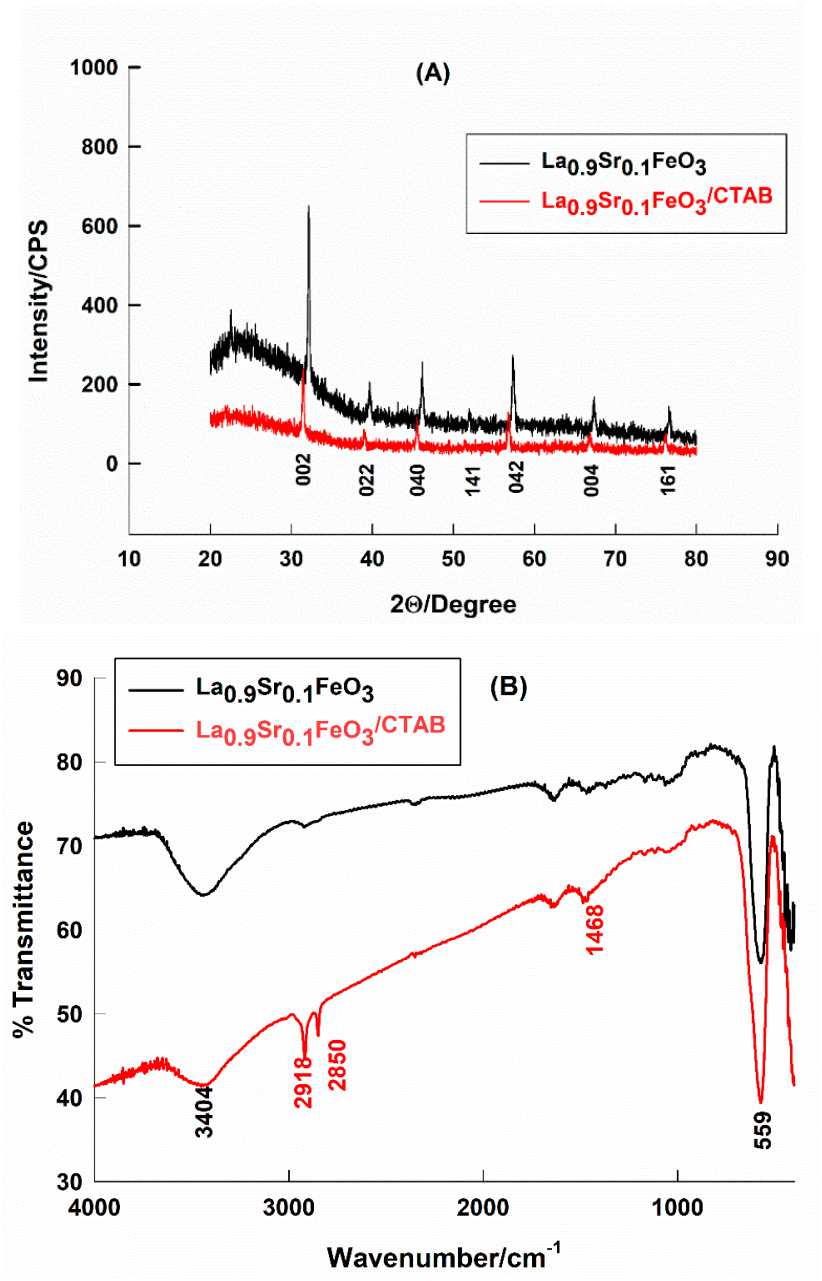

Figure 1. XRD patterns (**A**) and FTIR spectra (**B**) of pure and CTAB-capped $La_{0.9}Sr_{0.1}FeO_3$. Corresponding Miller indices and wavenumbers are indicated.

The measured BET surface area values for pure and CTAB-capped $La_{0.9}Sr_{0.1}FeO_3$ were 3.9 and 2.3 $m^2 \cdot g^{-1}$, respectively. The CTAB modification decreased the perovskite surface area.

The surface morphology of prepared samples was studied by SEM. Figure 2 shows SEM images of pure and CTAB-capped $La_{0.9}Sr_{0.1}FeO_3$ samples. The pure $La_{0.9}Sr_{0.1}FeO_3$ consisted of an interconnected bone-like network, Figure 2A. Upon the surfactant modification, SEM imaging, Figure 2B, shows that perovskite grains were more conjoined, thereby reducing interfacial spaces, as compared to the pure

sample, Figure 2A. This clearly showed the decreased porosity and, therefore, the decreased surface area of the perovskite by the modification with CTAB.

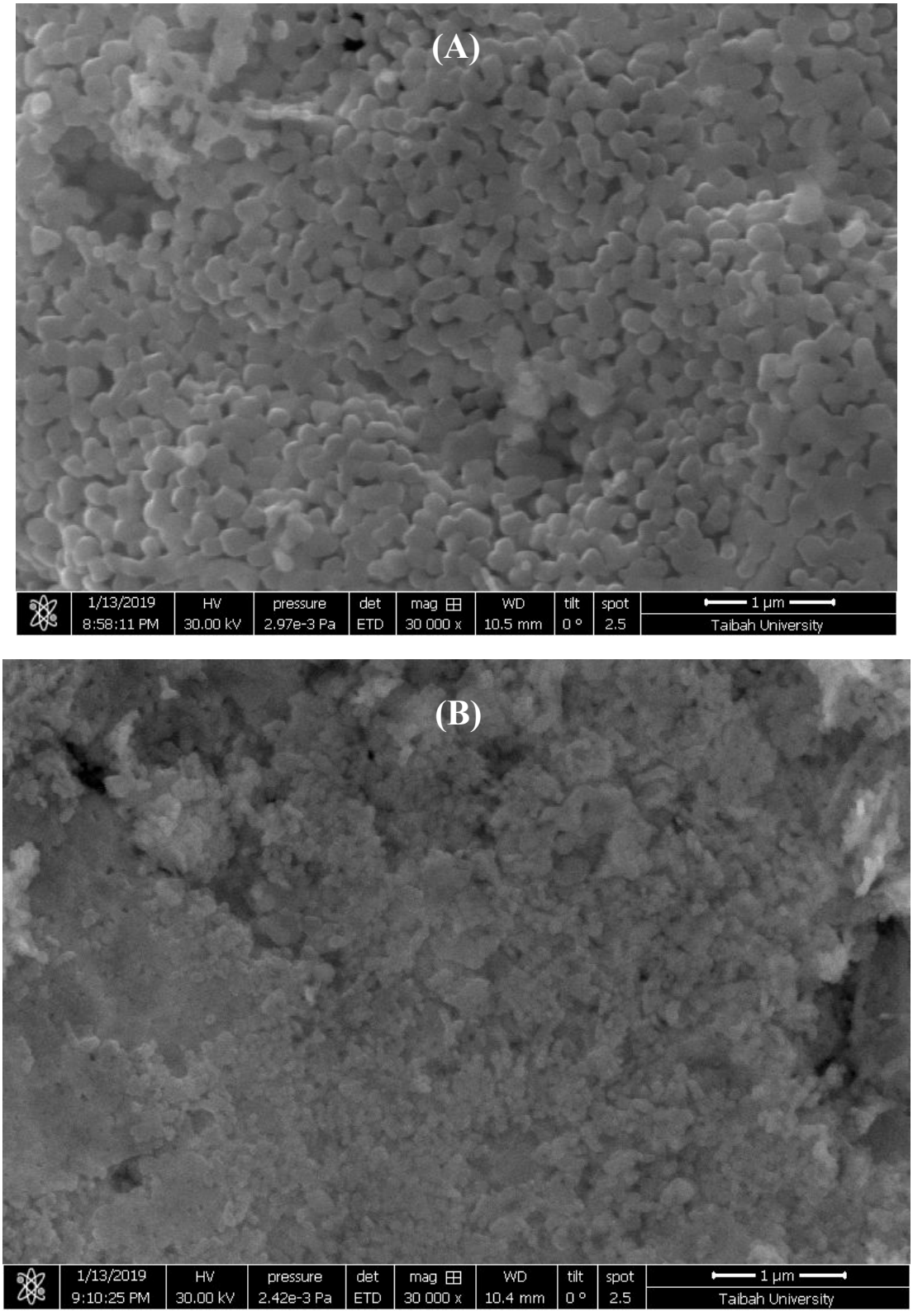

Figure 2. SEM images of pure (**A**), and CTAB-capped $La_{0.9}Sr_{0.1}FeO_3$ (**B**), with 30,000 times magnification.

2.2. *Application of CTAB-capped $La_{0.9}Sr_{0.1}FeO_3$ Perovskite as a Sorbent for CR Dye*

The absorption characteristic of the non-adsorbed CR dye in the solution was different when different sorbents were used—pure and CTAB-capped $La_{0.9}Sr_{0.1}FeO_3$ perovskites. Figure 3 shows the visible spectrum of the remaining CR dye, non-adsorbed in the solution, after batch experiments were performed using different sorbents. In the case of using the pure $La_{0.9}Sr_{0.1}FeO_3$, the visible spectrum was normal with a maximum wavelength, λ_{max}, of 498 nm, as reported in the literature [26]. On the other hand, the use of CTAB-capped $La_{0.9}Sr_{0.1}FeO_3$ resulted in a decreased λ_{max} value, at 466 nm, showing a hipsochromic shift. CR dye is an anionic dye, while CTAB is a cationic surfactant; therefore, an oppositely charged dye–surfactant complex is formed. This can cause a dye dimerization in the presence of the surfactant and a decrease in the dye absorbance value. It was reported that the dye dimerization could occur at a high dye concentration or in the presence of large molecules [44]. It can be seen that in the presence of CTAD—the surfactant-capped perovskite—the absorbance value of the non-adsorbed CR dye was largely decreased compared to that of the pure perovskite sorbent, which reflected the enhanced sorption ability of $La_{0.9}Sr_{0.1}FeO_3$ for the anionic CR dye as a result of being capped with a cationic CTAB surfactant.

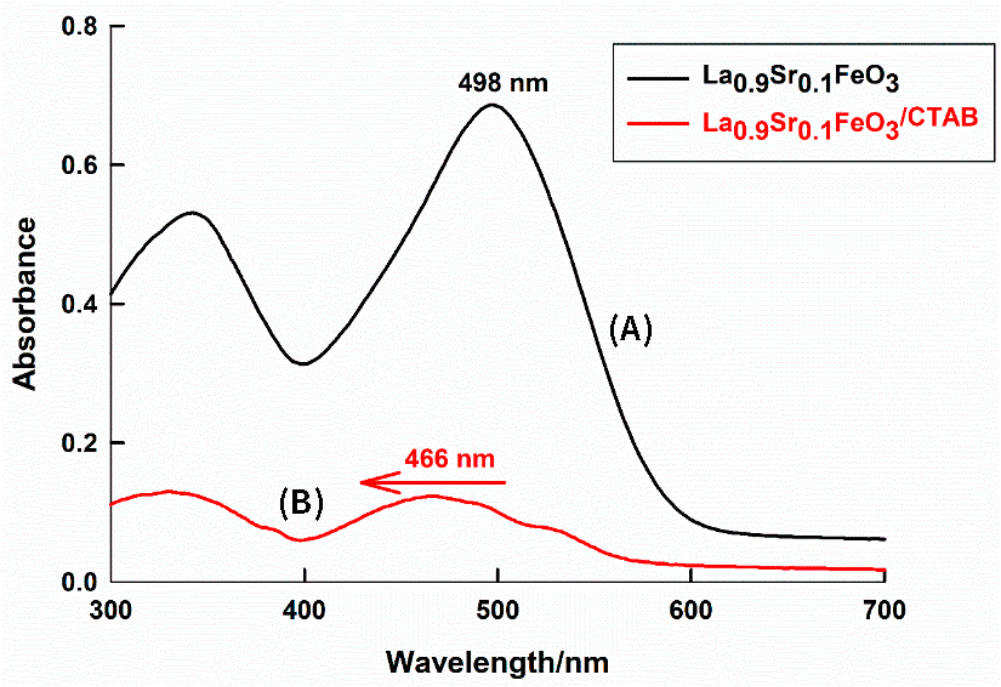

Figure 3. Visible absorption spectra of remaining CR dye in solutions by using (**A**) pure, and (**B**) CTAB-capped $La_{0.9}Sr_{0.1}FeO_3$ sorbents at pH = 6, the dye concentration = 10 ppm, contact time = 24 h, at 25 °C.

2.2.1. Effect of pH on the Adsorption Performance

It is well known that the pH value can greatly affect the removal efficiency of a sorbent. For most perovskites, the point of zero charge is about 5 [26,31]. Therefore, the perovskite is positively charged at pH < 5, and it is expected to have its highest sorption ability for the anionic dye under acidic conditions. Figure 4. shows the dependence of the removal % of CTAB-capped $La_{0.9}Sr_{0.1}FeO_3$ for CR on the pH of the dye solution. It can be shown that the adsorption performance was independent of the pH. A high value of the removal % was noticed at any pH value. This can be explained on the basis that the positively charged CTAB-perovskite sorbent can attract the negatively charged CR dye regardless of the pH value. Therefore, the proposed sorbent is suitable to be used in applications as it possesses a superior performance, irrespective of the operating pH. In the next sections, the optimum pH value will be taken to be 6, since it is close to neutral conditions and shows a removal % of 98.8%.

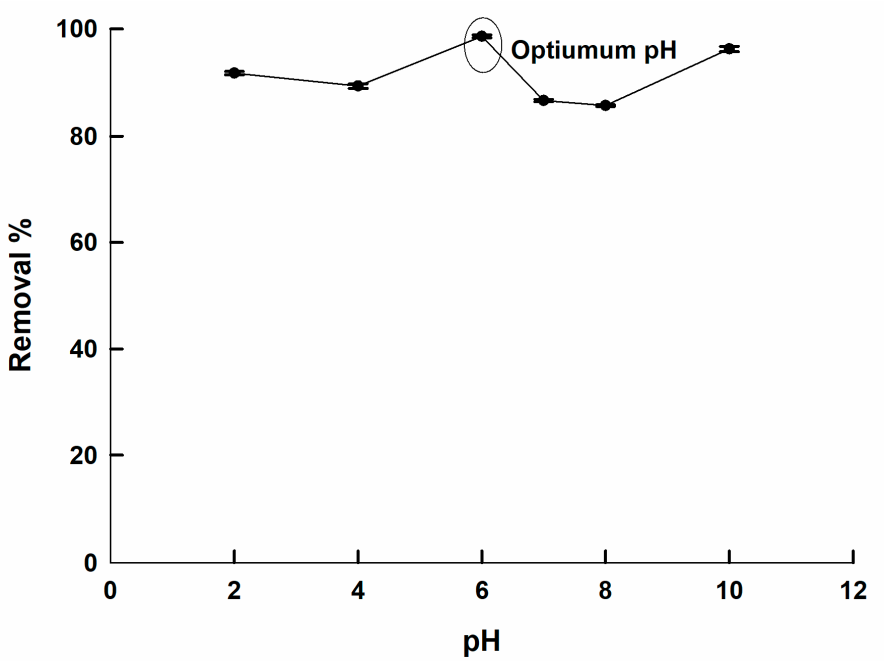

Figure 4. The relation between the CR removal % of by CTAB-capped $La_{0.9}Sr_{0.1}FeO_3$ and the solution pH, the dye concentration = 30 ppm, contact time = 24 h, at 25 °C.

2.2.2. Kinetic Study

The effect of the contact time was examined by estimating the adsorbed dye concentrations at different times, extended to 2 h, to identify the equilibrium position and to investigate the kinetics of the adsorption process. Figure 5A shows the relation between the removal % of CR by CTAB-capped $La_{0.9}Sr_{0.1}FeO_3$ and the contact time. It can be shown that the equilibrium is reached very fast, the removal % is ~97% at the start of the experiment. This reflected the possibility of applying the present sorbent in the field use, as it offered a rapid dye uptake.

The 1st and 2nd order models are given by Equations (1) and (2), respectively [45–48]:

$$\log(q_e - q_t) = log q_e - \frac{K_1}{2.303} t \quad (1)$$

$$\frac{t}{q_t} = \frac{1}{K_2 q_e} + \frac{t}{q_e} \quad (2)$$

where q_e, q_t were the adsorbed amounts in mg·g^{-1} at equilibrium, and at time t (min), respectively. K_1 and K_2 were first- and second-order rate constants, respectively.

It was found that the adsorption data did not fit the pseudo 1st order model at all, while it perfectly fitted the pseudo 2nd order model, as shown in Figure 5B. This implied that the surface reaction between the positively charged surfactant-capped perovskite and the negatively charged dye was the rate-determining step rather than the adsorption of dye on the sorbent active sites. In addition, it reflected the possibility of a dynamic equilibrium between the adsorbate and surface sites during the diffusion through the sorbent pores [49]. The experimental q_e value calculated from the pseudo 2nd order model matches well with the theoretical value, 5.21 and 5.16 mg·g^{-1}, respectively. The calculated value of the rate constant, K_2, was 0.42 g·mg^{-1}·min^{-1}.

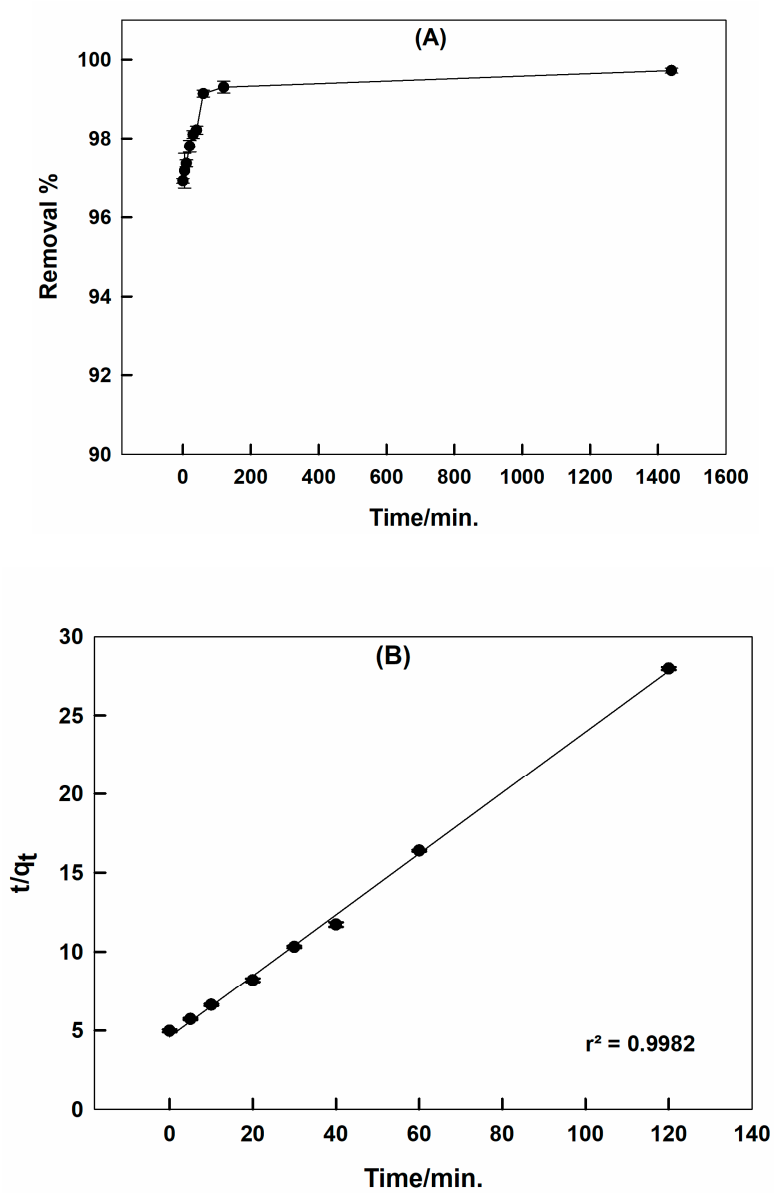

Figure 5. The relation between the CR removal % by CTAB-capped $La_{0.9}Sr_{0.1}FeO_3$ and the contact time; pH = 6, the dye concentration = 30 ppm, at 25 °C (**A**), and pseudo 2nd order model (**B**).

2.2.3. The Effect of the Initial Dye Concentration

Batch experiments were conducted by using different initial dye concentrations, 10–100 ppm, to examine the effect of the dye concentration. Figure 6A shows the relation between the removal % and the initial concentration of CR dye; the removal % increased as the dye concentration increased.

Adsorption data were fitted to Langmuir and Freundlich isotherms to deduce the mechanism of adsorption and to estimate the maximum adsorption capacity, q_m, of CTAB-capped $La_{0.9}Sr_{0.1}FeO_3$ for CR dye. Langmuir and Freundlich isotherms can be expressed by the following equations, respectively [35,45–48]:

$$\frac{C_e}{q_e} = \frac{1}{q_m b} + \frac{C_e}{q_m} \quad (3)$$

$$lnq_e = lnK_f + \frac{1}{n} lnC_e \quad (4)$$

where b was Langmuir constant, K_f and n were Freundlich isotherm constants.

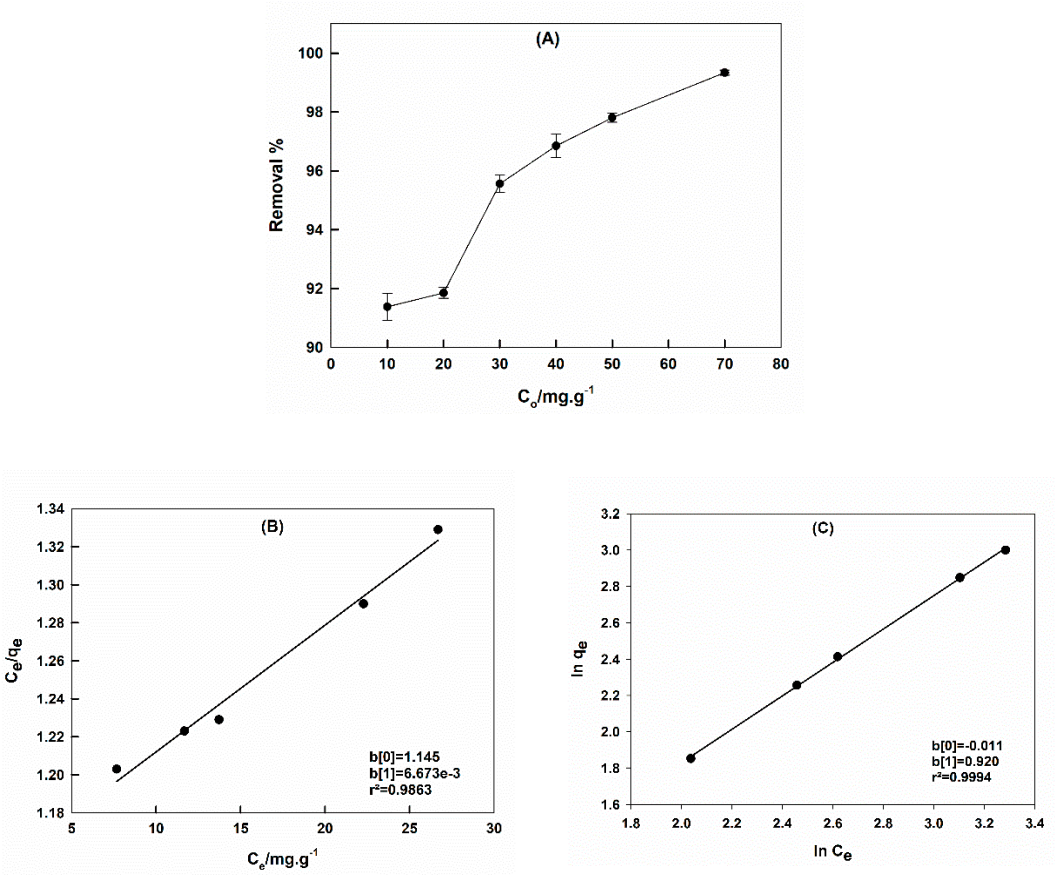

Figure 6. The relation between the CR removal by CTAB-capped $La_{0.9}Sr_{0.1}FeO_3$ and the initial CR concentration; pH = 6, contact time = 1 h, at 25 °C (**A**). Langmuir (**B**) and (**C**) Freundlich isotherms.

Figure 6B,C represent Langmuir and Freudlich isotherms, respectively. Correlation coefficient values were 0.9863 and 0.9994, respectively. This showed that the adsorption data were better fitted using the Freundlich isotherm, i.e., the CR adsorption was a monolayer on heterogeneous sites of the CTAB-capped perovskite. The calculated q_m value was 151.52 mg·g^{-1}. In a previous study, Ali and Al-Oufi reported the q_m value of pure $La_{0.9}Sr_{0.1}FeO_3$ as 13.89 mg·g^{-1} [26], indicating that CTAB modification enhanced the sorption performance of $La_{0.9}Sr_{0.1}FeO_3$ for CR dye by approximately 10 times. Despite the decreased particle size, surface area, and porosity of the perovskite upon surfactant capping, the CTAB-capped sample showed a superior adsorption ability with respect to the pure perovskite.

The calculated value of the Langmuir constant, b, was 0.0058 L·mg^{-1}, and the Freundlich constants, K_f and n, were 0.99 and 1.09, respectively. The separation factor, R_L, (dimensionless) can be calculated from the following equation [35]:

$$R_L = \frac{1}{1 + bC_o} \quad (5)$$

The value of R_L can indicate whether the adsorption was favored or not, where $R_L = 0$ (irreversible), $1 > R_L > 0$ (favored adsorption), $R_L = 1$ (linear), and $R_L > 1$ (unfavorable). The calculated R_L value was 0.63, which indicated the favorable adsorption of CR dye on the CTAB-capped $La_{0.9}Sr_{0.1}FeO_3$ perovskite.

2.2.4. The Adsorption Mechanism

The proposed adsorption mechanism involved three steps: (1) the electrostatic attractions between the positively charged CTAB heads and the negatively charged perovskite surface, forming a monolayer of CTAB-capped perovskite with tails pointed outwards. (2) Formation of a surfactant bilayer through tail–tail hydrophobic interactions, with positively charged heads pointed outwards.

(3) Strong electrostatic attractions between positively charged heads and negatively charged CR dye [37], Scheme 1.

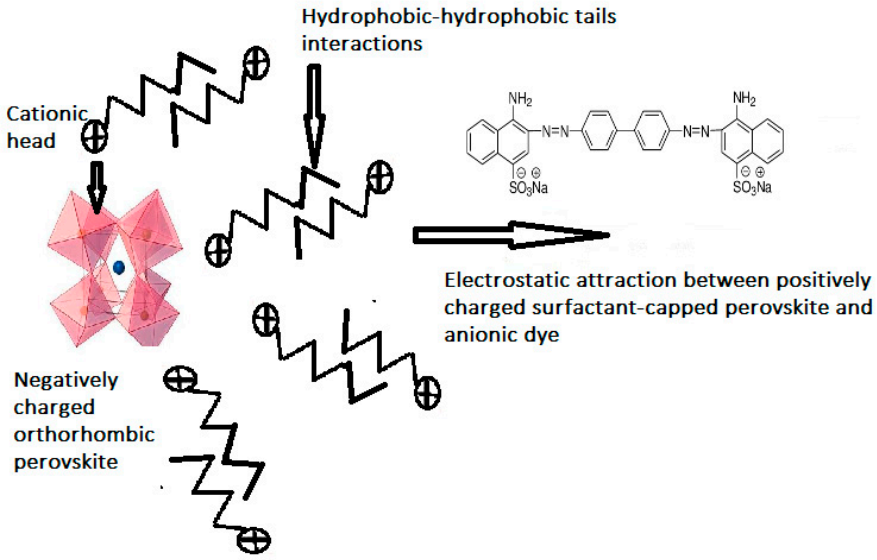

Scheme 1. Represented CR Adsorption mechanism by CTAB-capped $La_{0.9}Sr_{0.1}FeO_3$.

In addition, a comparison with other CTAB-capped sorbents for CR dye is presented in Table 1. It can be shown that CTAB-capped $La_{0.9}Sr_{0.1}FeO_3$ perovskite exhibited a considerable high-sorption performance. Although it did not show the highest q_m value among the CTAB-modified materials presented, the proposed sorbent maintained its high performance at all pH values and showed a rapid dye uptake.

Table 1. A comparison of the sorption performance of CTAB-capped $La_{0.9}Sr_{0.1}FeO_3$ with reported CTAB-modified materials for the CR removal.

Sorbent	q_m (mg·g^{-1})	Optimum pH Conditions	Equilibrium Time/min.	Reference
CTAB-chitosan beads	94.4	Acidic	240	[35]
CTAB-chitosan hydrogel beads	433.1	Acidic	240	[36]
CTAB-Tea waste	106.4	Independent	30	[37]
CTAB-Hectorite	182.0	Independent	120	[38]
CTAB-Kaolin	24.5	Alkaline	10	[39]
Bentonite-CTAB	210.0	Independent	90	[40]
graphene oxide-CTAB	2767.0	Acidic	60	[41]
CTAB-$La_{0.9}Sr_{0.1}FeO_3$	**151.5**	**Independent**	**Less than 5**	**This work**

The sorption performance of the proposed sorbent for CR dye in the presence of a real sample matrix, taken from factory wastewater in Cairo, Egypt, was investigated. The calculated q_m value was 143.23 mg·g^{-1}; therefore, CTAB-capped perovskite maintained its excellent performance despite the matrix interferences.

2.2.5. Temperature Effect

Figure 7A shows the dependence of the removal % of CTAB-capped $La_{0.9}Sr_{0.1}FeO_3$ for CR on temperature. The removal % continued to increase with the temperature increase.

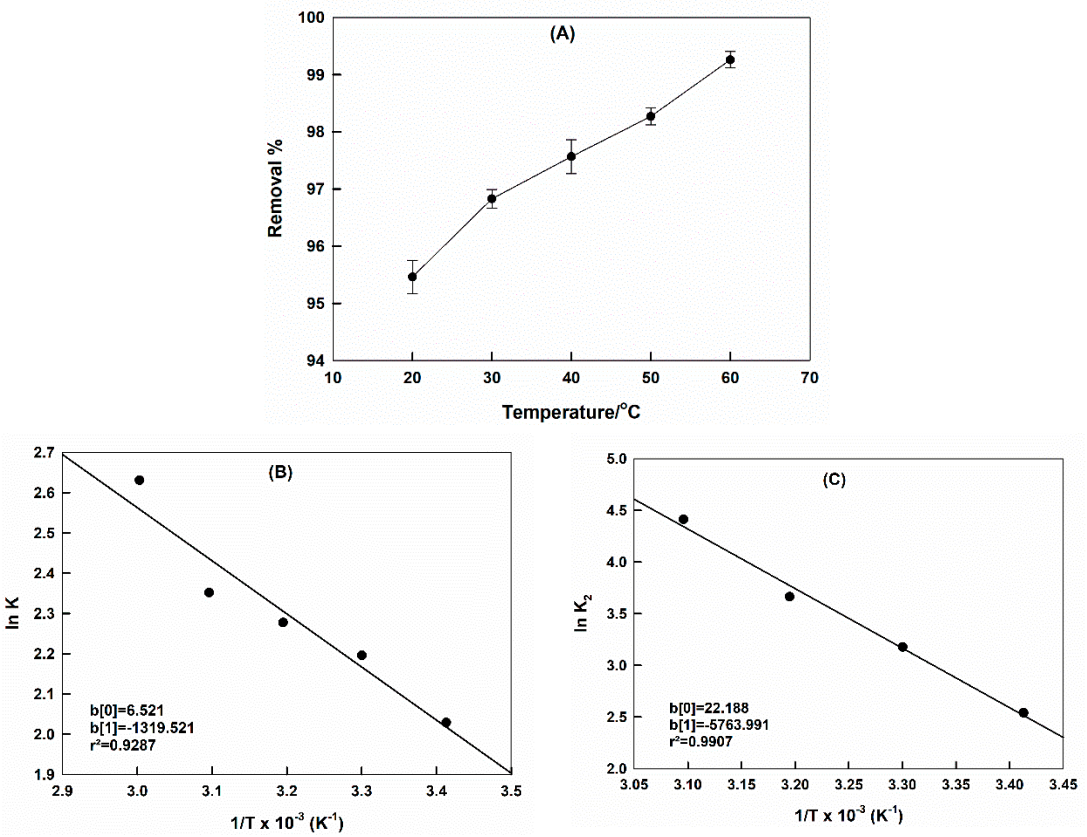

Figure 7. The relation between CR removal by CTAB-capped $La_{0.9}Sr_{0.1}FeO_3$ with temperature; pH = 6, the dye concentration = 30 ppm, contact time = 1 h (**A**), transition-state (**B**), and Arrhenius (**C**) plots.

Standard enthalpy and entropy changes, ΔH^o and ΔS^o, therefore, can be calculated by constructing the transition-state plot, according to the transition-state equation [35,45–48]:

$$\ln K = \frac{\Delta S^o}{R} - \frac{\Delta H^o}{R}\left(\frac{1}{T}\right) \quad (6)$$

$$K = \frac{C_{Ad}}{C_e} \quad (7)$$

where K was the equilibrium constant, C_{Ad} and C_e were concentrations of adsorbed dye on the sorbent and non-adsorbed dye in solution, respectively.

The transition-state plot is shown in Figure 7B. Calculated values of ΔH^o and ΔS^o were 10.95 kJ·mol^{-1} and 54.12 J·mol^{-1}·K^{-1}, respectively. This indicated that the adsorption is exothermic and the disorder is increased by the adsorption of CR on the CTAB-capped perovskite surface.

The value of the standard Gibbs free energy change, ΔG^o, can be calculated using the following equation:

$$\Delta G^o = \Delta H^o - T\Delta S^o \quad (8)$$

The calculated ΔG^o value, was −4.91 kJ·mol^{-1}, i.e., a spontaneous adsorption at room temperature.

The value of the activation energy, E_a, can be calculated from the slope of the Arrhenius plot, which is shown in Figure 7C. The value was found to be 47.84 kJ·mol^{-1}, which indicated that the adsorption of CR on CTAB-capped $La_{0.9}Sr_{0.1}FeO_3$ perovskite is a chemisorption—it involved an electrostatic attraction between the positively charged sorbent and the negatively charged dye [26].

2.2.6. The Sorption Performance by Repeated Use and its Regeneration

CTAB-capped $La_{0.9}Sr_{0.1}FeO_3$ perovskite was used for several cycles to examine its sorption ability with repeated use. Figure 8 shows the change of the removal % for CR dye with the number of use cycles, indicated by the black columns. The removal % is decreased from 98.8 to 83.5% after the 5th cycle, indicating a removal efficiency decrease by about 15.5% after five operating cycles. This reflected an acceptable performance of CTAB-capped $La_{0.9}Sr_{0.1}FeO_3$ sorbent.

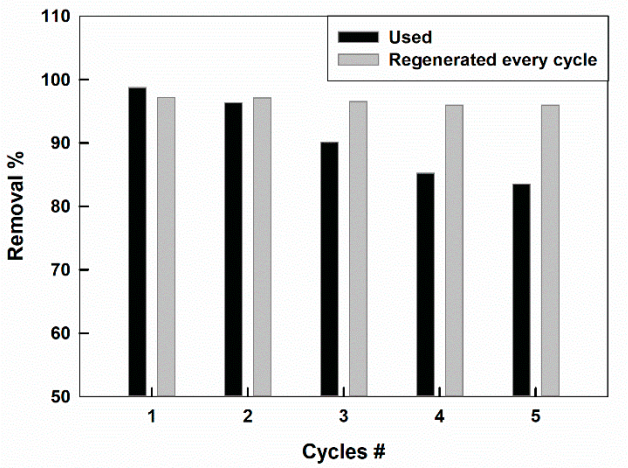

Figure 8. The removal % of (black) used and (gray) regenerated CTAB-capped $La_{0.9}Sr_{0.1}FeO_3$ as a function of the number of use cycles.

A possible sorbent regeneration can be performed by stirring the used sorbent in 1 mmol L^{-1} of aqueous surfactant solution for 1 h, before each use. The change of the removal % with the number of use cycles for the regenerated sorbent, is shown by the gray columns in Figure 8. It can be shown that the regenerated sorbent maintained its excellent performance even after five cycles of use, as indicated by the unchanged removal % values.

3. Materials and Method

3.1. Materials

$La(NO_3)_3{\cdot}6H_2O$ (99.9%), $Fe(NO_3)_3{\cdot}9H_2O$ (99.9%), $Sr(NO_3)_2$ (99.9%), and $C_6H_8O_7$ (99%), NH_4OH (33%), HNO_3 (65%), and CTAB (99%) were purchased from Sigma Aldrich. CR dye, $C_{32}H_{22}N_6Na_2O_6S_2$ (Brixworth, Northants, United Kingdom). All chemicals were used as-received.

3.2. Microwave-assisted Citrate Combustion Synthesis of $La_{0.9}Sr_{0.1}FeO_3$ Perovskite

$La(NO_3)_3{\cdot}6H_2O$, $Sr(NO_3)_2$, and $Fe(NO_3)_3{\cdot}9H_2O$ were mixed in a molar ratio of 0.9:0.1:1.0, and dissolved in distilled water. Citric acid was added to the metal ion solution, the pH value of which was previously adjusted to 8, at the same ratio to that of the total metal ions. The mixture was heated until combustion occurred in a microwave oven (700 watt for 30 min.). The resultant black powder was calcined at 900 °C for 3 h [26]. CTAB capping was performed by immersing the final calcined powder in 1 mmol L^{-1} of aqueous CTAB solution for 1 h with stirring.

3.3. Adsorption Test

A quantity of 0.05 g CTAB-capped perovskite/25 mL dye solution was shaken at 150 rpm for 1 d at an ambient temperature. The solution was then centrifuged at 3500 rpm for 1h. The concentration of the remaining, non-adsorbed dye was calculated by measuring the absorbance of clear solution by the UV-Vis spectrometer (Evolution 300, United Kingdom) at λ_{Max} of 466 nm.

The removal % of the CR dye can be estimated according to the following equation [44–48]:

$$\text{Removal } \% = \frac{C_o - C_e}{C_o} \times 100 \quad (9)$$

The adsorbed CR amount, at the equilibrium, q_e (mg g^{-1}), was calculated from the following:

$$q_e = \frac{(C_o - C_e)\text{V}}{\text{W}} \quad (10)$$

where C_o and C_e were the initial and equilibrium concentrations of the dye (mg L^{-1}), V was the solution volume (L) and W was the sorbent mass (g).

Uncertainties of adsorption experiment parameters were listed in Table S1.

3.4. Characterization Instruments

X-ray diffractograms were used for the phase identification (XRD-7000, Shimadzu), at 40 kV and 30 mA, using a CuK_α incident beam (λ = 0.154 nm). FTIR spectroscopy was used for identification of characteristic functional groups, (IRAffinity-1S, Shimadzu).

Scanning electron microscopy was used to examine the surface morphology (Superscan SS-550, Shimadzu), with an accelerating voltage = 25 kV.

Micromeritics ASAP 2020 was used to evaluate Brunauer–Emmet–Teller (BET) surface area values, with N_2 adsorption isotherms at −196 °C at a relative pressure (P/P_o) of 0.2.

4. Conclusions

$La_{0.9}Sr_{0.1}FeO_3$ can be successively capped with a cationic surfactant CTAB. The capping did not alter the perovskite chemical structure but resulted in a larger particle size with decreased porosity and BET surface area. CTAB-capped $La_{0.9}Sr_{0.1}FeO_3$ can be used as an excellent sorbent for anionic CR dye, due to the formation of an oppositely charged dye–CTAB complex. The proposed sorbent has many advantages over reported CTAB-capped sorbents; it maintained its high performance at any pH value, showed fast dye uptake, and the removal % was high—approximately 97% at the start of the adsorption. The adsorption followed the Freundlich isotherm, which indicated a monolayer chemical adsorption of CR dye on heterogeneous CTAB-capped perovskite sites. The calculated q_m value was 151.52 mg·g^{-1}, which was 10 times higher than that of the pure perovskite. The calculated E_a value was 47.84 kJ·mol^{-1}, reflecting a chemical surface reaction. CTAB-capped $La_{0.9}Sr_{0.1}FeO_3$ also showed an unaffected performance in the presence of the sample matrix, q_m = 143.23 mg·g^{-1}, which highly recommended it for applications in the field. It can be easily regenerated with unchanged removal ability, thus, offering an economic benefit.

Supplementary Materials: The following are available online, Table S1: Uncertainties of adsorption experiment parameters.

Author Contributions: S.M.A. designed, performed the experiments, and analyzed the data; S.M.A. and A.A.E. contributed reagents/materials/analysis tools; S.M.A. wrote the paper; S.M.A. and A.A.E. revised and approved submitted paper. All authors have read and agreed to the published version of the manuscript.

Funding: This research received no external funding.

Conflicts of Interest: The authors declared that they have no conflict of interest.

References

1. Knepper, T.P.; Berna, J.L. Chapter 1 Surfactants: Properties, production, and environmental Aspects. *Compr. Anal. Chem.* **2003**, *40*, 1–49.
2. Heinz, H.; Pramanik, C.; Heinz, O.; Ding, Y.; Mishra, R.K.; Marchon, D.; Flatt, R.J.; Estrela-Lopis, I.; Llop, J.; Moya, S.; et al. Nanoparticle decoration with surfactants: Molecular interactions, assembly, and applications. *Surf. Sci. Rep.* **2017**, *72*, 1–58. [CrossRef]

3. Emran, K.M.; Ali, S.M.; Al-Oufi, A.L.L. Synthesis and characterization of nano-conducting copolymer composites: Efficient sorbents for organic pollutants. *Molecules* **2017**, *22*, 772. [CrossRef] [PubMed]
4. Bakshi, M.S. How Surfactants Control Crystal Growth of Nanomaterials. *Cryst. Growth. Des.* **2016**, *162*, 1104–1133. [CrossRef]
5. Kim, D.K.; Zhang, Y.; Voit, W.; Rao, K.V.; Muhammed, M. Synthesis and characterization of surfactant-coated superparamagnetic monodispersed iron oxide nanoparticles. *J. Magn. Magn. Mater.* **2001**, *225*, 30–36. [CrossRef]
6. Elfeky, S.A.; Mahmoud, S.E.; Youssef, A.F. Applications of CTAB modified magnetic nanoparticles for removal of chromium (VI) from contaminated water. *J. Adv. Res.* **2017**, *8*, 435–443. [CrossRef] [PubMed]
7. Li, N.; Fu, F.; Lu, J.; Ding, Z.; Tang, B.; Pang, J. Facile preparation of magnetic mesoporous MnFe2O4@SiO2–CTAB composites for Cr(VI) adsorption and reduction. *Environ. Pollut.* **2017**, *220*, 1376–1385. [CrossRef]
8. Zhao, B.; Xiao, W.; Shang, Y.; Zhu, H.; Han, R. Adsorption of light green anionic dye using cationic surfactant-modified peanut husk in batch mode. *Arab. J. Chem.* **2017**, *10*, S3595–S3602. [CrossRef]
9. Malik, M.A.; Hashim, M.A.; Nabi, F.; AL-Thabaiti, S.A.; Khan, Z. Anti-corrosion ability of surfactants: A review. *Int. J. Electrochem. Sci.* **2011**, *6*, 1927–1948.
10. Sliem, M.H.; Afifi, M.; Radwan, A.B.; Fayyad, E.M.; Shibl, M.F.; Heakal, F.E.T.; Abdullah, A.M. AEO7 Surfactant as an Eco-Friendly Corrosion Inhibitor for Carbon Steel in HCl solution. *Sci Rep.* **2019**, *9*, 2319. [CrossRef]
11. Migahed, M.A.; Al-Sabagh, A.M. Beneficial role of surfactants as corrosion inhibitors in petroleum industry. *Chem. Eng. Commun.* **2009**, *196*, 1054–1075. [CrossRef]
12. Zahid, A.; Lashin, A.; Rana, U.A.; Al-Arifi, N.; Ullah, I.; Dionysiou, D.D.; Qureshi, R.; Waseem, A.; Kraatz, H.B.; Shah, A. Development of surfactant based electrochemical sensor for the trace level detection of mercury. *Electrochim. Acta.* **2016**, *190*, 1007–1014. [CrossRef]
13. Manjunatha, J.G. Surfactant modified carbon nanotube paste electrode for the sensitive determination of mitoxantrone anticancer drug. *J. Electrochem. Sci. Eng.* **2017**, *7*, 39–49. [CrossRef]
14. Zhu, L.; Cao, Y.; Cao, G. Electrochemical sensor based on magnetic molecularly imprinted nanoparticles at surfactant modified magnetic electrode for determination of bisphenol A. *Biosens. Bioelectron.* **2014**, *54*, 258–261. [CrossRef] [PubMed]
15. Khan, A.F.; Brownson, D.A.C.; Foster, C.W.; Smith, G.C.; Banks, C.E. Surfactant exfoliated 2D hexagonal Boron Nitride (2D-hBN) explored as a potential electrochemical sensor for dopamine: Surfactants significantly influence sensor capabilities. *Analyst* **2017**, *142*, 1756–1764. [CrossRef]
16. Almora-Barrios, N.; Vilé, G.; Garcia-Ratés, M.; Pérez-Ramírez, J.; López, N. Electrochemical Effects at Surfactant–Platinum Nanoparticle Interfaces Boost Catalytic Performance. *ChemCatChem* **2017**, *9*, 604–609. [CrossRef]
17. Wang, Z.; Liu, P.; Han, J.; Cheng, C.; Ning, S.; Hirata, A.; Fujita, T.; Cen, M. Engineering the internal surfaces of three-dimensional nanoporous catalysts by surfactant-modified dealloying. *Nat. Commun.* **2017**, *8*, 1066. [CrossRef]
18. Ma, C.; Chen, Y.; Chen, J. Surfactant-assisted preparation of FeCu catalyst for Fischer-Tropsch synthesis. *J. Braz. Chem. Soc.* **2015**, *26*, 1520–1526. [CrossRef]
19. Hu, N.; Rusling, J.F. Surfactant-Intercalated Clay Films for Electrochemical Catalysis. Reduction of Trichloroacetic Acid. *Anal. Chem.* **1991**, *63*, 2163–2168. [CrossRef]
20. Rusling, J.F. Controlling Electrochemical Catalysis with Surfactant Microstructures. *Acc. Chem. Res.* **1991**, *24*, 75–81. [CrossRef]
21. Assirey, E.A. Perovskite synthesis, properties and their related biochemical and industrial application. *Saudi Pharm. J.* **2019**, *27*, 817–829. [CrossRef]
22. Kulkarni, S.A.; Mhaisalkar, S.G.; Mathews, N.; Boix, P.P. Perovskite Nanoparticles: Synthesis, Properties, and Novel Applications in Photovoltaics and LEDs. *Small Methods* **2019**, *3*, 1800231. [CrossRef]
23. Atta, N.F.; Galal, A.; Ali, S.M. The effect of the lanthanide ion-type in $LnFeO_3$ on the Catalytic activity for the Hydrogen evolution in acidic medium. *Int. J. Electrochem. Sci.* **2014**, *9*, 2132–2148.
24. Ali, S.M.; Abdel Al-Rahman, Y.M.; Galal, A. Catalytic activity toward oxygen evolution of $LaFeO_3$ prepared by the microwave assisted citrate method. *J. Electrochem. Soc.* **2012**, *159*, F600–F605. [CrossRef]

25. Ali, S.M.; Abdel Al-Rahman, Y.M. Catalytic activity of $LaBO_3$ for OER in $HClO_4$ medium: An approach to the molecular orbital theory. *J. Electrochem. Soc.* **2016**, *163*, H81–H88. [CrossRef]
26. Ali, S.M.; Al-Oufi, B. A Synergistic Sorption Capacity of $La_{0.9}Sr_{0.1}FeO_3$ Perovskite for Organic Dyes by Cellulose Modification. *Cellulose* **2020**, *27*, 429–440. [CrossRef]
27. Luu, M.D.; Dao, N.N.; Nguyen, D.V.; Pham, N.C.; Vu, T.N.; Doan, T.D. A new perovskite-type $NdFeO_3$ adsorbent: Synthesis, characterization, and As(V) adsorption. *Adv. Nat. Sci. Nanosci. Nanotechnol.* **2016**, *7*, 025015–025027. [CrossRef]
28. Tavakkoli, H.; Yazdanbakhsh, M. Fabrication of two perovskite-type oxide nanoparticles as the new adsorbents in efficient removal of a pesticide from aqueous solutions: Kinetic, thermodynamic, and adsorption studies. *Microporous Mesoporous Mater.* **2013**, *176*, 86–94. [CrossRef]
29. Carmen, Z.; Daniel, S. Textile Organic Dyes Characteristics, Polluting Effects and Separation/Elimination Procedures from Industrial Effluents–A Critical Overview. In *Organic Pollutants Ten Years after Stockholm Convention, Environmental and Analytical Update*; InTech: Rijeka, Croatia, 2012.
30. Srilakshmi, C. Microwave Synthesis of Perovskite Based High Surface Area $SrTiO_3$ Nanoparticles: Application for Adsorption of Congo Red Dye in Water. *Nano. Lett.* **2018**, *2*, 10–15.
31. Bhagya, N.P.; Prashanth, P.A.; Raveendra, R.S.; Sathyanarayani, S.; Ananda, S.; Nagabhushana, B.M.; Nagabhushana, H. Adsorption of hazardous cationic dye onto the combustion derived $SrTiO_3$ nanoparticles: Kinetic and isotherm studies. *J. Asian Ceram. Soc.* **2016**, *4*, 68–74. [CrossRef]
32. Farhadi, S.; Mahmoudi, F.; Amini, M.M.; Dusek, M.; Jarosova, M. Synthesis and characterization of a series of novel perovskite-type $LaMnO_3$/Keggin-type polyoxometalate hybrid nanomaterials for fast and selective removal of cationic dyes from aqueous solutions. *Dalt. Trans.* **2017**, *46*, 3252–3264. [CrossRef] [PubMed]
33. Tavakkoli, H.; Beiknejad, D.; Tabari, T. Fabrication of perovskite-type oxide $La_{0.5}Ca_{0.5}CoO_3-\delta$ nanoparticles and its Dye removal performance. *Desalin. Water Treat.* **2014**, *4*, 116–125.
34. Yazdanbakhsh, M.; Tavakkoli, H.; Hosseini, S.M. Characterization and evaluation catalytic efficiency of $La_{0.5}Ca_{0.5}NiO_3$ nanopowders in removal of reactive blue 5 from aqueous solution. *Desalination* **2011**, *281*, 388–395. [CrossRef]
35. Shadeera, R.; Nagapadma, M.; Ramakoteswara, R. Removal of Harmful Textile Dye Congo Red from Aqueous Solution Using Chitosan and Chitosan Beads Modified with CTAB. *J. Eng. Res. Appl.* **2015**, *5*, 75–82.
36. Chatterjee, S.; Lee, D.S.; Lee, M.W.; Woo, S.H. Enhanced adsorption of congo red from aqueous solutions by chitosan hydrogel beads impregnated with cetyl trimethyl ammonium bromide. *Bioresour. Technol.* **2009**, *100*, 2803–2809. [CrossRef]
37. Foroughi-Dahr, M.; Abolghasemi, H.; Esmaieli, M.; Nazari, G.; Rasem, B. Experimental study on the adsorptive behavior of Congo red in cationic surfactant-modified tea waste. *Process Saf. Environ. Prot.* **2015**, *95*, 226–236. [CrossRef]
38. Xia, C.; Jing, Y.; Jia, Y.; Yue, D.; Ma, J.; Yin, X. Adsorption properties of congo red from aqueous solution on modified hectorite: Kinetic and thermodynamic studies. *Desalination* **2011**, *265*, 81–87. [CrossRef]
39. Zenasni, M.A.; Meroufel, B.; Merlin, A.; George, B. Adsorption of Congo Red from Aqueous Solution Using CTAB-Kaolin from Bechar Algeria. *J. Surf. Eng. Mater. Adv. Technol.* **2014**, *4*, 332–341. [CrossRef]
40. Youssef, A.M.; Al-Awadhi, M.M. Adsorption of Acid Dyes onto Bentonite and Surfactant-modified Bentonite. *J. Anal. Bioanal. Tech.* **2013**, *4*, 1–7. [CrossRef]
41. Su, J.; He, S.; Zhao, Z.; Liu, X.; Li, H. Efficient preparation of cetyltrimethylammonium bromide-graphene oxide composite and its adsorption of Congo red from aqueous solutions. *Colloids Surfaces A Physicochem. Eng. Asp.* **2018**, *554*, 227–236. [CrossRef]
42. Muniz, F.T.L.; Miranda, M.A.R.; Santos, C.M.D.; Sasaki, J.M. The Scherrer equation and the dynamical theory of X-ray diffraction. *Acta Crystallogr. Sect. A Found. Adv. A* **2016**, *72*, 385–390. [CrossRef] [PubMed]
43. Su, G.; Yang, C.; Zhu, J.J. Fabrication of gold nanorods with tunable longitudinal surface plasmon resonance peaks by reductive dopamine. *Langmuir* **2015**, *31*, 817–823. [CrossRef] [PubMed]
44. Bielska, M.; Sobczyńska, A.; Prochaska, K. Dye-surfactant interaction in aqueous solutions. *Dye Pigments* **2009**, *80*, 201–205. [CrossRef]
45. Ahmed, M.A.; Ali, S.M.; El-Dek, S.I.; Galal, A. Magnetite-hematite nanoparticles prepared by green methods for heavy metal ions removal from water. *Mater. Sci. Eng. B Solid-State Mater. Adv. Technol.* **2013**, *178*, 741–755. [CrossRef]

46. Ali, S.M.; Emran, K.M.; Al-Oufi, A.L.L. Adsorption of organic pollutants by nano-conducting polymers composites: Effect of the supporting nano-oxide type. *J. Mol. Liq.* **2017**, *233*, 89–99. [CrossRef]
47. Ali, S.M.; Galal, A.; Atta, N.F.; Shammakh, Y. Toxic heavy metal ions removal from wastewater by nano-magnetite: Case study nile river water. *Egypt J. Chem.* **2017**, *60*, 601–612. [CrossRef]
48. Ali, S.M. Fabrication of a nanocomposite from an agricultural waste and its application as a biosorbent for organic pollutants. *Int. J. Environ. Sci. Technol.* **2018**, *15*, 1169–1178. [CrossRef]
49. Hubbe, M.A.; Azizian, S.; Douven, S. Implications of apparent pseudo-second-order adsorption kinetics onto cellulosic materials: A review. *BioResources* **2019**, *14*, 7582–7626.

Sample Availability: Samples of the compounds, pure and CTAB-capped $La_{0.9}Sr_{0.1}FeO_3$ perovskites are available from the authors.